Optical potential study of positron scattering by atomic sodium at intermediate energies

Nithyanandan Natchimuthu and Kuru Ratnavelu
Quantum Scattering Theory Group, Institute of Mathematical Sciences, University of Malaya, 50603 Kuala Lumpur, Malaysia
(Received 2 October 2000; published 13 April 2001)

The coupled-channel optical method has been applied to study positron scattering by atomic sodium at intermediate energies. The optical potential that accounts only for the continuum has been implemented into the close-coupling framework and includes positron–sodium-atom and the positronium–sodium-ion channels. Elastic, excitation, ionization, positronium formation, and total cross sections are reported and are compared with other theoretical and experimental data, where available.

DOI: 10.1103/PhysRevA.63.052707 PACS number(s): 34.10.+x, 34.90.+q

I. INTRODUCTION

Much work using optical potentials has been done to study electron (e^-) scattering from atoms. Among them, the coupled-channel optical method (CCOM) of McCarthy and Stelbovics [1] has been extensively used to study e^- scattering from a number of atoms. The CCOM has also been used to study positron (e^+) scattering with atoms [2,3]. However, these calculations did not include the positronium (Ps) channels explicitly into the calculations.

It was only in the last decade that a resurgence of theoretical studies on e^+-H scattering systems has been observed due to major advances in treating the Ps channels explicitly for $n>1$, with Ps channels coupled to the H atom [4–16]. These calculations have provided the most realistic investigations for e^+-H scattering. Since alkali-metal atoms have a relatively simple structure (a single valence e^- on the outer shell) and can be simplified into a three-body scattering problem, there has been a natural extension of these theoretical calculations from the scattering of e^+-H to e^+–alkali-metal atoms [12,17–22].

The first realistic calculation on the e^+-Na scattering system was done by Hewitt *et al.* [17] using the coupled-channel (CC) method with four atomic states of Na($3s$,$3p$,$4s$,$4p$) coupled to the Ps($n=1$) and Ps($n=2$) states. However, there were some technical details in this work that were not resolved [18]. Subsequently, Mitroy and Ratnavelu [18] investigated the e^+-Na scattering system using five atomic states ($3s$,$3p$,$4s$,$3d$,$4p$) coupled to the Ps($n=1$) and Ps($n=2$) and also included the effects of the core using a core potential model. An extension to this work was done by Ryzhikh and Mitroy [19] where the Ps basis states were enlarged to include Ps($n=3$) and Ps($n=4$) states. McAlinden and co-workers have also done extensive calculations on almost the entire alkali-metal series using the *R*-matrix approach and this can be seen in their numerous works [12,20–22]. Their work on e^+-Na only included the Na($3s$,$3p$) coupled with the Ps($n=1$) and Ps($n=2$) states [12].

Ray *et al.* [23] have suggested that the exclusion of the exchange interaction between the core electrons and the electron in the Ps molecule by Mitroy and Ratnavelu [18] may play a role and should be included for the e^+-Na and other positron–alkali-metal scattering systems. Their work was performed within the first-order Born approximation (FBA) and they also conclude that their work is very limited. Since then, we are unaware of any work reported by Ghosh and co-workers on this aspect. Later, Ryzhikh and Mitroy [19] have shown for e^+-Na scattering that the exclusion of the core has a minor effect of around 3–4 % on the cross sections at 10 eV. They have argued that the repulsive nature of the positron-nucleus potential would probably have little effect on the positron-sodium entrance channel. In the higher energies, the core exchange may be an important effect, but then there is less possibility of Ps formation. Thus they summarized that the inclusion of the core exchange would be unlikely to have a significant impact on their results. In the large-scale *R*-matrix calculations by McAlinden and co-workers [20–22], we note that the core-direct effect is represented by an approximate potential and they do not allow for the core-exchange effects. Recently, we have also seen a convergent close-coupling (CCC) calculation [24] for e^+-Li that used 46 states, which does not even take into account the Ps channels for the intermediate-energy regions. The CCC results were in good agreement with the work of McAlinden *et al.* [20] above 6 eV. We believe that the neglect of the core exchange may be a reasonable approximation that would not affect the calculation of gross physical parameters such as the cross sections. A particular work to note is the highly successful CCC work of Bray [25] for corresponding e^--Na scattering. The CCC has achieved unparallel successes with respect to the calculations of various cross sections and the highly sensitive spin-exchange asymmetry parameters by using only a simple phenomenological polarization potential to allow for core exchange and virtual excitation of the core. We believe that in the present work, which is an extension of the method of Mitroy and co-workers [18,19], the exclusion of the exchange between the core electrons and the electron in the Ps molecule is a reasonable approximation.

In this work, the e^+-Na scattering system is studied at the energy regime that encompasses the energy region from the ionization threshold to approximately ten times of this threshold. The CCOM was used by McCarthy *et al.* [3] for e^+-Na scattering calculations. However, their work did not allow for the explicit inclusion of the Ps–Na-ion channels in the coupled-channel equation. It was only recently that e^+-H scattering calculations using the CCOM with the Ps channels explicitly coupled to the H atom was done by Ratnavelu and

Rajagopal [26]. Their work has shown much success in comparison with other theoretical works and experimental measurements [26,27]. Their calculations using a small basis states with continuum optical potentials shows comparable cross sections with the larger L^2 models of Mitroy [9] and Kernoghan *et al.* [15]. Thus, it is only natural to extend the CCOM to e^+–alkali-metal atoms as there are very few theoretical calculations for e^+–alkali-metal atom scattering systems. The Na atom became an obvious choice due to the availability of some experimental data [28–30] and other calculations for comparison [18,19].

II. THEORETICAL DETAILS

The full theoretical details of the close-coupling (CC) formulation for e^+-Na can be found in Mitroy and Ratnavelu [18]. Here, only the main outline of the CC method and the details of the optical potential will be given.

A. The coupled-channel approach

The following notations are used. Ψ denotes the bound atomic states of the Na atom, ϕ denotes the bound state of the Ps molecule, and Ω denotes the ionic state of the Na atom. The subscripts α and β will be used to separate between the manifolds of the atomic and Ps states. The three assumptions made by Mitroy and Ratnavelu are as follows.

(1) Only the valence electron will be removed from the Na atom to form the Ps molecule.

(2) Exchange interaction between the electron in the Ps molecule with the rest of the electrons in the ion core is neglected.

(3) The fixed-core model is used to compute the wave functions for the atomic and the ionic state of Na. This then reduces the many-body problem into an effective three-body problem.

Following the notational details of Mitroy and Ratnavelu [18] and Ryzhikh and Mitroy [19], we write $\mathbf{r}_0$ and $\mathbf{r}_i$, $i \in \{1,2,...,N\}$ as the coordinate of the incoming positron and the electron in sodium, respectively, and $r_{i0}=|\mathbf{r}_i-\mathbf{r}_0|$ is the distance between the positron and the electron. By using the relative ($\boldsymbol{\rho}_i$) and center-of-mass coordinates ($\mathbf{R}_i$) for any Ps channels, the relation between the coordinates can be written as

$$\boldsymbol{\rho}_i=\mathbf{r}_i-\mathbf{r}_0, \quad \mathbf{R}_i=\frac{1}{2}(\mathbf{r}_i+\mathbf{r}_0),$$

$$\mathbf{r}_i=\mathbf{R}_i+\frac{1}{2}\boldsymbol{\rho}_i, \quad \mathbf{r}_0=\mathbf{R}_i-\frac{1}{2}\boldsymbol{\rho}_i.$$

The total wave function of the system (e^+-Na) is expanded in an eigenfunction expansion of the positron scattering states $F_\alpha(\mathbf{r}_0)$, and the Ps states $\phi_\beta(\boldsymbol{\rho})$, which are coupled to the atomic states $\psi_\alpha(\mathbf{r}_i)$ and the ionic state $\Omega(\mathbf{r}_{i'})$ (the valence electron is denoted by $i=1$), and written as

$$\Psi(\mathbf{r}_i,\mathbf{r}_0)=\sum_\alpha \psi_\alpha(\mathbf{r}_i)F_\alpha(\mathbf{r}_0)+\sum_\beta \Omega(\mathbf{r}_{i'})\phi_\beta(\boldsymbol{\rho}_1)G_\beta(R_1). \tag{1}$$

The Schrödinger equation is given by

$$(H-E)\Psi(\mathbf{r}_i,\mathbf{r}_0)=0. \tag{2}$$

The Hamiltonian H in the Schrödinger equation can be partitioned into (for a $N+1$ system)

$$(H_e+H_{\text{atom}}-E)\Psi(\mathbf{r}_i,\mathbf{r}_0)=0, \tag{3}$$

where

$$H_e=-\frac{1}{2}\nabla_0^2+\frac{Z}{r_0}-\sum_{i=1}^{N}\frac{1}{\mathbf{r}_{i0}}, \tag{4}$$

$$H_{\text{atom}}=\sum_{i=1}^{N}\left(-\frac{1}{2}\nabla_i^2-\frac{Z}{r_i}\right)+\frac{1}{2}\sum_{\substack{i=1\\ i\neq j}}^{N}\frac{1}{r_{ij}}. \tag{5}$$

An alternative partitioning of the Hamiltonian in the Schrödinger equation, incorporating Ps formation is given as (writing $\boldsymbol{\rho}_1=\boldsymbol{\rho}$ and $\mathbf{R}_1=\mathbf{R}$)

$$(H_{\text{Ps}}+H_{\text{int}}+H_{\text{ion}}-E)\Psi(\boldsymbol{\rho},\mathbf{R},\mathbf{r}_{i'})=0, \tag{6}$$

where

$$H_{\text{int}}=-\nabla_{\boldsymbol{\rho}}^2+\frac{1}{r_{10}}, \tag{7}$$

$$H_{\text{ion}}=\sum_{i=2}^{N}\left(-\frac{1}{2}\nabla_i^2-\frac{Z}{r_i}\right)+\frac{1}{2}\sum_{\substack{i,j=2\\ i\neq j}}^{N}\frac{1}{r_{ij}}, \tag{8}$$

and

$$H_{\text{Ps}}=-\frac{1}{4}\nabla_{\mathbf{R}}^2+\frac{Z}{r_0}-\frac{Z}{r_1}-\sum_{i=2}^{N}\left(\frac{1}{r_{i0}}-\frac{1}{r_{i1}}\right). \tag{9}$$

The states Ψ_α, ϕ_β, and Ω satisfy the equations

$$\langle\Psi_\alpha(\mathbf{r}_i)|H_{\text{atom}}-\varepsilon_\alpha|\Psi_\alpha(\mathbf{r}_i)\rangle=0, \tag{10}$$

$$\langle\phi_\beta(\boldsymbol{\rho})|H_{\text{int}}-\varepsilon_\beta|\phi_\beta(\boldsymbol{\rho})\rangle=0, \tag{11}$$

and

$$\langle\Omega(\mathbf{r}_{i'})|H_{\text{ion}}-\varepsilon_{\text{core}}|\Omega(\mathbf{r}_{i'})\rangle=0. \tag{12}$$

ε_α is the energy of the atomic state, ε_β is the energy of the Ps species, and $\varepsilon_{\rm core}$ is the energy of the closed-shell core. It can then be shown that

$$\left(E+\frac{1}{2}\nabla_0^2-\varepsilon_{\alpha'}-\varepsilon_{\rm core}\right)F_{\alpha'}(\mathbf{r}_0)=\sum_\alpha \langle\Psi_{\alpha'}(\mathbf{r}_i)|\left(\frac{Z}{r_0}-\sum_{i=1}^{N}\frac{1}{r_{0i}}\right)\Psi_\alpha(\mathbf{r}_i)F_\alpha(\mathbf{r}_0)+\sum_\beta \langle\Psi_{\alpha'}(\mathbf{r}_i)\times|(H-E)|\Omega(\mathbf{r}_{i'})\phi_\beta(\boldsymbol{\rho})G_\beta(\mathbf{R})\rangle \tag{13}$$

and

$$\left(E+\frac{1}{4}\nabla_{\mathbf{R}}^2-\varepsilon_{\beta'}-\varepsilon_{\rm core}\right)G_{\beta'}(\mathbf{R})=\sum_\alpha \langle\phi_{\beta'}(\boldsymbol{\rho})\Omega(\mathbf{r}_{i'})|(H-E)|\Psi_\alpha(\mathbf{r}_i)F_\alpha(\mathbf{r}_0)\rangle+\sum_\beta \langle\phi_{\beta'}(\boldsymbol{\rho})\Omega(\mathbf{r}_{i'})|\times\left[\frac{Z}{r_0}-\frac{Z}{r_1}-\sum_{i=2}^{N}\left(\frac{1}{r_{i0}}-\frac{1}{r_{i1}}\right)\right]|\phi_\beta(\boldsymbol{\rho})\Omega(\mathbf{r}_{i'})\rangle G_\beta(\mathbf{R}). \tag{14}$$

Using Eqs. (13) and (14), the momentum-space Lippmann-Schwinger (LS) equations for a positron with momentum $\mathbf{k}$ on a Na atom in the state $\Psi_\alpha(\mathbf{r}_i)$ can be written as

$$\langle\mathbf{k}'\Psi_{\alpha'}|T|\mathbf{k}\Psi_\alpha\rangle=\langle\mathbf{k}'\Psi_{\alpha'}|V|\mathbf{k}\Psi_\alpha\rangle+\sum_{\alpha''}\int d^3k''\frac{\langle\mathbf{k}'\Psi_{\alpha'}|V|\mathbf{k}''\Psi_{\alpha''}\rangle\langle\mathbf{k}''\Psi_{\alpha''}|T|\mathbf{K}\psi_\alpha\rangle}{E^{(+)}-\varepsilon_{\alpha''}-\varepsilon_{\rm core}-\frac{1}{2}k''^2}+\sum_{\beta''}\int d^3k''\frac{\langle\mathbf{k}'\Psi_{\alpha'}|V|\mathbf{k}''\Omega\phi_{\beta''}\rangle\langle\mathbf{k}''\Omega\phi_{\beta''}|T|\mathbf{k}\Psi_\alpha\rangle}{E^{(+)}-\varepsilon_{\beta''}-\varepsilon_{\rm core}-\frac{1}{4}k''^2},$$

$$\langle\mathbf{k}'\Omega\phi_{\beta'}|T|\mathbf{k}\Psi_\alpha\rangle=\langle\mathbf{k}'\Omega\phi_{\beta'}|V|\mathbf{k}\Psi_\alpha\rangle+\sum_{\alpha''}\int d^3k''\frac{\langle\mathbf{k}'\Omega\phi_{\beta'}|V|\mathbf{k}''\Psi_{\alpha''}\rangle\langle k''\Psi_{\alpha''}|T|\mathbf{k}\Psi_\alpha\rangle}{E^{(+)}-\varepsilon_{\alpha''}-\varepsilon_{\rm core}-\frac{1}{2}k''^2}+\sum_{\beta''}\int d^3k''\frac{\langle\mathbf{k}'\Omega\phi_{\beta'}|V|\mathbf{k}''\Omega\phi_{\beta''}\rangle\langle\mathbf{k}''\Omega\phi_{\beta''}|T|\mathbf{k}\Psi_\alpha\rangle}{E^{(+)}-\varepsilon_{\beta''}-\varepsilon_{\rm core}-\frac{1}{4}k''^2}. \tag{15}$$

The generic term V is used to label the interaction between different classes of channels and the details can be found in Mitroy and Ratnavelu [18].

B. Details of the optical potential method

In the present work we have implemented the CCOM of McCarthy and Stelbovics [1] to study e^+–alkali-metal atoms. This is an extension to a previous work by Ratnavelu and Rajagopal [26] for e^+-H scattering system. Here, only a brief outline of the derivation of the momentum-space form of the optical potential for the continuum using the Feshbach projection-operator formalism will be given [1]. The Hamiltonian for e^+-Na can be written as

$$H=K_1+K_2+\nu_1+\nu_2+\nu_{12}. \tag{16}$$

K_1 and K_2 stand for the kinetic energy of the incoming e^+ and the valence e^-, respectively. ν_1 and ν_2 are the e^+-core and e^--core potential operators. ν_{12} is the e^+-e^- potential operator. Spin-orbit coupling is ignored here, implying that the e^- spin plays a role only at the application of the Pauli exclusion principle. The Schrödinger equation for the total energy E is

$$(E-H)\Psi_n=0, \tag{17}$$

where Ψ_n is the total three-body wave function of the collision system and the number n denotes the three-body quantum state with respect to quantum numbers of bound state and momenta of the valence e^- and the incoming e^+. The space of reaction channels is divided into two orthogonal or complementary subspaces by means of the projection operators P and Q. The P space consists of the finite set of the discrete channels used in the close-coupling theory and the Q space comprises the remaining discrete channels and the continuum, and they are defined as

$$P=\sum_{i\in P}|\psi_i\rangle\langle\psi_i| \tag{18}$$

and

$$Q=\sum_{j\in Q}|\psi_j\rangle\langle\psi_j|, \tag{19}$$

where ψ_i is the asymptotic ''free'' state vectors describing the system in the state i in a particular rearrangement channel. The operators operate on the three-body wave function $|\Psi_n\rangle$. In principle, Eq. (18) should incorporate the Ps states, ϕ_β. In this work, however, the Ps states are neglected and the optical potential approach is used to allow for only the atomic and the continuum space of Na. From the projection-operator definition, we have

$$Q=\mathbf{1}-P,$$

$$P^2=P, \quad Q^2=Q,$$

$$PQ=QP=\mathbf{0}. \tag{20}$$

With these above definitions, it is easily shown that

$$P(E-K-\nu_2-V^{(Q)})P\Psi_n=0. \tag{21}$$

with

$$V^{(Q)}=V_1+V_2, \tag{22}$$

where

$$V_1=\nu_1+\nu_{12}, \tag{23}$$

$$V_2=(\nu_1+\nu_{12})Q\frac{1}{Q(E-K-v)Q}Q(\nu_1+\nu_{12}). \tag{24}$$

Thus, Eq. (21) is an approximation to the original Schrödinger equation appearing in Eq. (17). The term V_1 is the first-order static-exchange potential and V_2 is the complex, nonlocal polarization potential. The V_2 term consists of a real part that describes virtual excitation into Q space and an imaginary part that describes real excitation into Q space. The V_2 potential is intractable and is localized using the localization procedure of McCarthy and Stelbovics [1]. Details of the optical potentials can be found in McCarthy and Stelbovics [1] and Rajagopal and Ratnavelu [27]. The calculation of the total ionization cross section is given by

$$\sigma_I=\frac{2}{P}(2\pi)^3W(0), \tag{25}$$

where $P=\sqrt{2E}$ [1] and W are the imaginary part of the optical potential matrix element (see Rajagopal and Ratnavelu [27]). The calculation of the total ionization cross section using Eq. (25) will be denoted as the continuum optical potential method (COPM). The full LS equations following the formalism of $V^{(Q)}$ are then given by

$$\begin{aligned}
\langle\mathbf{k}'\Psi_{\alpha'}|T|\mathbf{k}\Psi_\alpha\rangle&=\langle\mathbf{k}'\Psi_{\alpha'}|V^{(Q)}|\mathbf{k}\Psi_\alpha\rangle+\sum_{\alpha''}\int d^3k''\frac{\langle\mathbf{k}'\Psi_{\alpha'}|V^{(Q)}|\mathbf{k}''\Psi_{\alpha''}\rangle\langle\mathbf{k}''\Psi_{\alpha''}|T|\mathbf{k}\Psi_\alpha\rangle}{E-\varepsilon_{\alpha''}-\varepsilon_{\rm core}-\frac{1}{2}k''^2}\\
&+\sum_{\beta''}\int d^3k''\frac{\langle\mathbf{k}'\Psi_{\alpha'}|V|\mathbf{k}''\Omega\phi_{\beta'}\rangle\langle\mathbf{k}''\Omega\phi_{\beta''}|T|\mathbf{k}\Psi_\alpha\rangle}{E-\varepsilon_{\beta''}-\varepsilon_{\rm core}-\frac{1}{4}k''^2},\\
\langle\mathbf{k}'\Omega\phi_{\beta'}|T|\mathbf{k}\Psi_\alpha\rangle&=\langle\mathbf{k}'\Omega\phi_{\beta'}|V|\mathbf{k}\Psi_\alpha\rangle+\sum_{\alpha''}\int d^3k''\frac{\langle\mathbf{k}'\Omega\phi_{\beta'}|V|\mathbf{k}''\Psi_{\alpha''}\rangle\langle\mathbf{k}''\Psi_{\alpha''}|T|\mathbf{k}\Psi_\alpha\rangle}{E-\varepsilon_{\alpha''}-\varepsilon_{\rm core}-\frac{1}{2}k''^2}\\
&+\sum_{\beta''}\int d^3k''\frac{\langle\mathbf{k}'\Omega\phi_{\beta'}|V|\mathbf{k}''\Omega\phi_{\beta''}\rangle\langle\mathbf{k}''\Omega\phi_{\beta''}|T|\mathbf{k}\Psi_\alpha\rangle}{E-\varepsilon_{\beta''}-\varepsilon_{\rm core}-\frac{1}{4}k''^2}.
\end{aligned} \tag{26}$$

Details of the numerical techniques for solving the LS equations can be found in the works of and Stelbovics [1], Mitroy [5], and Ratnavelu *et al.* [16].

C. Testing the continuum

Basically, the quality of our model continuum optical model can be gauged by its prediction of the ionization cross section. However, there are no ionization cross-section measurements of e^+-Na available for comparison up to the present. Thus, we compare the COPM ionization cross section with the theoretical calculation of Mukherjee *et al.* [31] (see Fig. 1). We find that there is good agreement between the COPM(e^+) and the calculations of Mukherjee *et al.*

To study the COPM in a better perspective, we also compare the predictions of the COPM for the e^--Na case with available experimental measurements of Johnston and Burrow [32] and other theoretical calculations, such as the CCC calculations of Bray [33] in Fig. 1. It can be observed that the e^--Na experimental measurements and the CCC are in good agreement with the COPM(e^-) calculations. This validates the quality of the COPM model for the e^--Na scattering system. Thus, it can be assumed that the COPM(e^+)

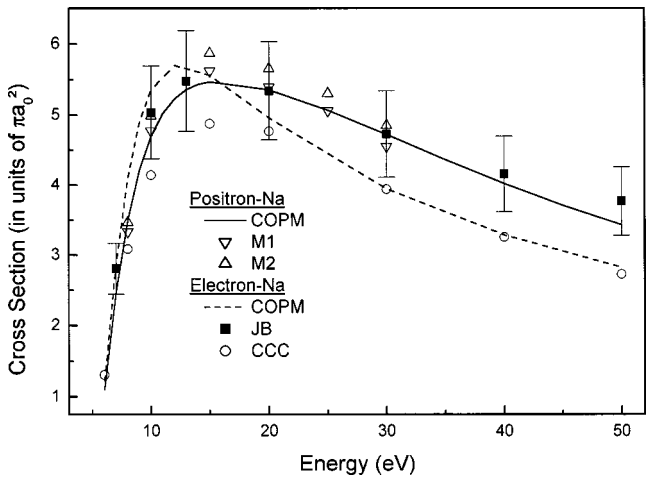

FIG. 1. Ionization cross section (in units of πa_0^2): COPM [(e^+-Na) (——), COPM (e^--Na) (— — —), Johnston and Burrow (■), CCC (○) and Mukherjee *et al.* $M1$ model (▽) and $M2$ model (△)].

may provide reasonable predictions of the ionization cross section for the e^+-Na scattering system.

III. RESULTS AND DISCUSSION

The following calculations were performed.

(i) CC(5,3): This CC calculation includes the Na($3s$,$3p$,$4s$,$3d$,$4p$) states together with the Ps($n=1$) and Ps($n=2$) states.

(ii) CCO(5,3): In this calculation, the nine states in (i) are used together with the continuum optical potentials for the $3s$-$3s$, $3p$-$3p$, $3s$-$3p$, $3s$-$4s$, and $3s$-$4p$ couplings.

All calculations were performed in the energy region of 5–50 eV. The higher partial waves for the Ps formation was excluded due to the time consuming nature of its calculation since they become difficult to handle as J increases [16]. The partial waves for the Ps channels were allowed only for $J \leqslant 16$ and the LS equations were solved. For $J > J_{\max}$, the unitarized Born approximation model is used (which is naturally obtained from the LS equations by discarding the off-shell part of the channel-free functions). For the CCO(5,3) calculations, the continuum optical potentials were allowed for $0 \leqslant J \leqslant J_{\text{opt}}$. The number of partial waves used in the calculations differs with the energy. For instance, at 7 eV, $J_{\max}$ is limited to only 18 while J_{opt} is taken up to ten partial waves. At 20 eV, the value of $J_{\max}$ used is 80 and J_{opt} is equal to 24. Whereas at 50 eV, $J_{\max}$ is equal to 100 and J_{opt} is equal to 36. For all calculations, a quadrature mesh of 48 points was used.

We also performed the CCO(5,0) calculations for e^+-Na with the same optical potentials used in (ii) at certain energies. These calculations, however, will only be discussed in the context of the ionization cross sections. For comparison with e^+-Na scattering processes, we have included calculations for the e^--Na scattering system at certain energies using the five-state CC model that includes the $3s$-$3s$, $3p$-$3p$, $3s$-$3p$, $3s$-$4s$, and $3s$-$4p$ optical potential couplings. These calculations will be denoted as the CCO5 calculations.

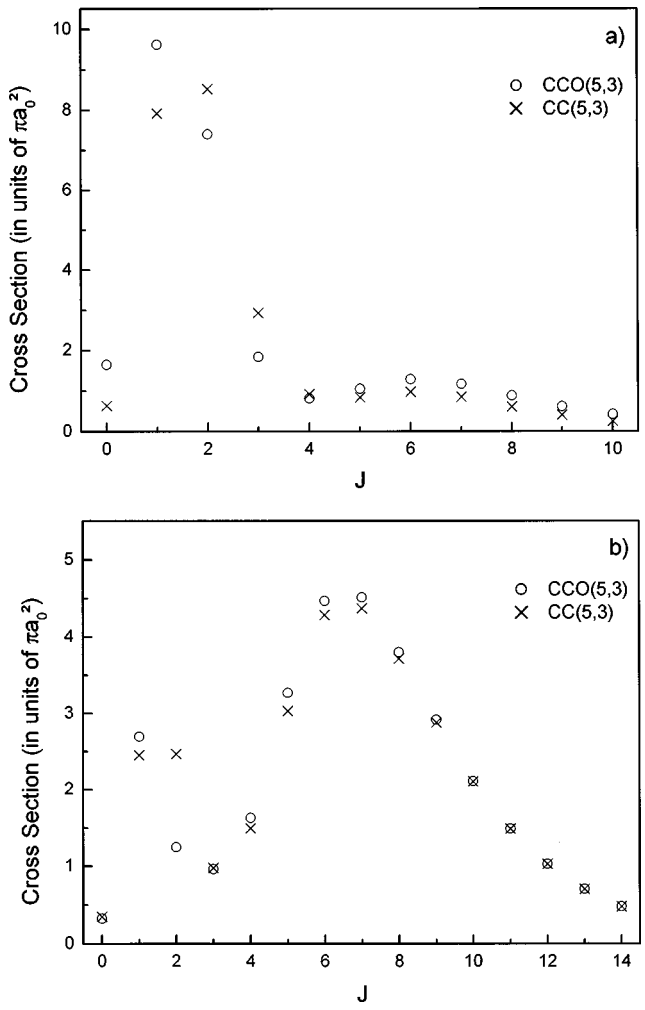

FIG. 2. Partial-wave cross sections at 7 eV. (a) Elastic. (b) $3s$-$3p$ transition: CCO(5,3) (○) and CC(5,3) (×).

A. Consistency of CC(m,n) and CCO(m,n) calculations

This work reports an extension of implementing the continuum optical potentials from e^+-H scattering of Ratnavelu and Rajagopal [26] to e^+-Na scattering. The optical potentials were implemented only for the e^+-Na discrete channels. In this section the consistency of these present calculations is evaluated by studying the partial-wave cross sections for the elastic and $3s$-$3p$ transition at 7 and 50 eV.

1. 7 eV

In Fig. 2(a) the elastic Na($3s \rightarrow 3s$) transition partial-wave cross sections are depicted at 7 eV. In the elastic case, all models show a tendency to converge for $J \geqslant 6$. Generally, the CCO(5,3) cross sections are larger than the CC(5,3) calculations except at $J=2$ and 3. For both the CC(5,3) and CCO(5,3) calculations, there is a presence of a resonance structure at $J=2$ and 3 and the largest contribution to the elastic cross section comes from these partial waves.

Figure 2(b) depicts the Na($3s \rightarrow 3p$) transition partial waves also at 7 eV. In this transition, convergence for all

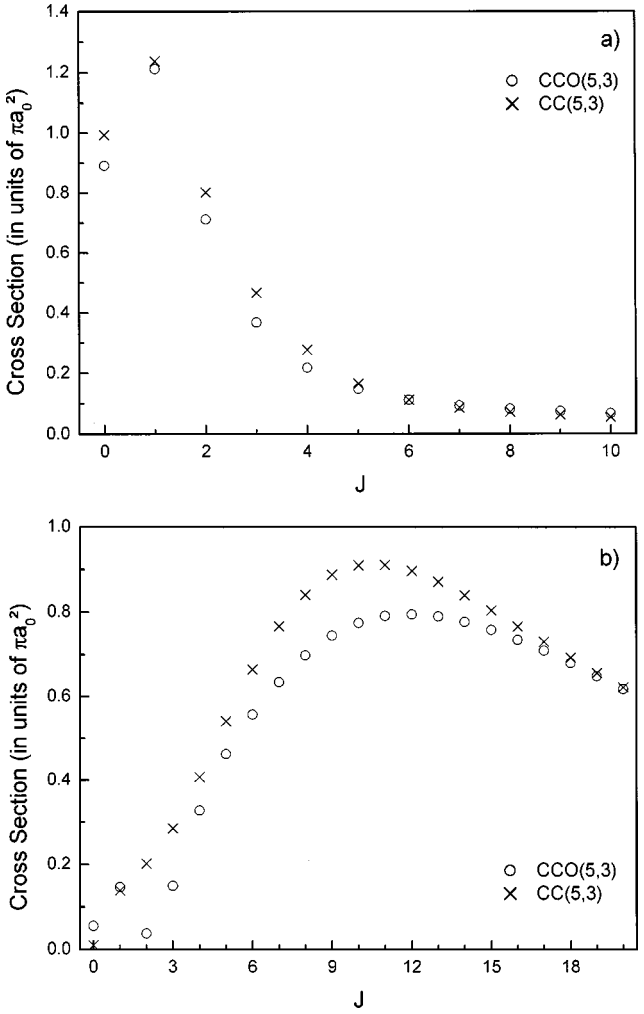

FIG. 3. Partial-wave cross sections at 50 eV. (a) Elastic. (b) $3s$-$3p$ transition: the legends are the same as those in Fig. 2.

models is only observed for $J \geqslant 10$. We also observe two structures at $J=1$ and 7 for both the CCO(5,3) and the CC(5,3) models. There are visible structures in the various transitions cross sections at around this energy region (see Figs. 5–7). Overall, the differences between the CC(5,3) and CCO(5,3) calculations do not exceed 10% with the exception at $J=2$, where the CC(5,3) is more than 50% larger than the CCO(5,3) calculations. However, the qualitative shapes are never distorted by the use of the optical potentials for the above transitions.

2. 50 eV

In Fig. 3(a) we show the partial-wave cross sections for the elastic Na($3s \rightarrow 3s$) transition at 50 eV. The qualitative shape of the partial-wave cross section observed for this transition is similar to the 7-eV case with the exception that there is no dip observed in this particular transition. For $0 \leqslant J \leqslant 4$, the partial-wave cross sections for the CCO(5,3) model are generally less than the CC(5,3) model. Beyond this, the CCO(5,3) tends to have larger cross sections than the CC(5,3) model. Convergence is observed for $J \geqslant 6$ for all models.

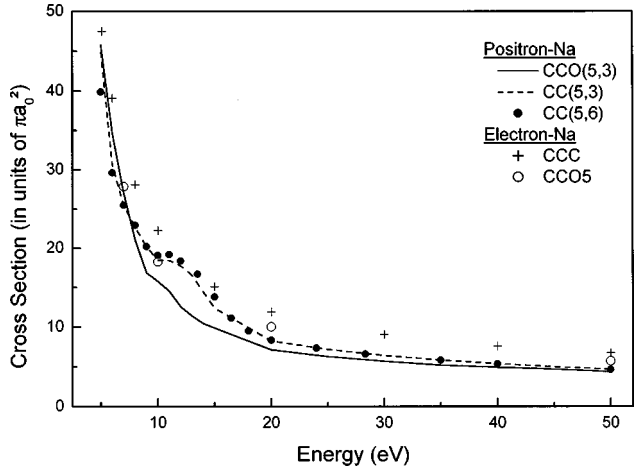

FIG. 4. Total elastic cross section (in units of πa_0^2): CCO(5,3) (——), CC(5,3) (– – –), CC(5,6) (●), CCO5, (×), and CCC (○).

In Fig. 3(b) the partial-wave cross section for the Na($3s \rightarrow 3p$) transition is depicted. Here, the qualitative shape of this transition at this energy is totally dissimilar to the 7-eV case. Both models tend to increase gradually and peak at $J=11$ and then decrease systematically. Convergence is only achieved at $J=20$. In this transition, the partial-wave cross sections for the CCO(5,3) model are smaller than the CC(5,3) at all partial waves except at $J=0$ and 1. Interestingly, adding the optical potentials tends to reduce the CCO(5,3) calculations at $J=2$, thus displaying some sort of resonance.

By investigating these two different energy spectrums, we find no outstanding abnormalities observed in the present CCO(5,3) calculations. This then provides a useful gauge of the correctness and the consistency of the present CCO(m,n) calculations.

B. Elastic and excitation cross section for the Na($3s$) entrance channel

In Figs. 4–8, elastic and excitation cross sections are compared with the cross sections calculated by the CC(5,6)

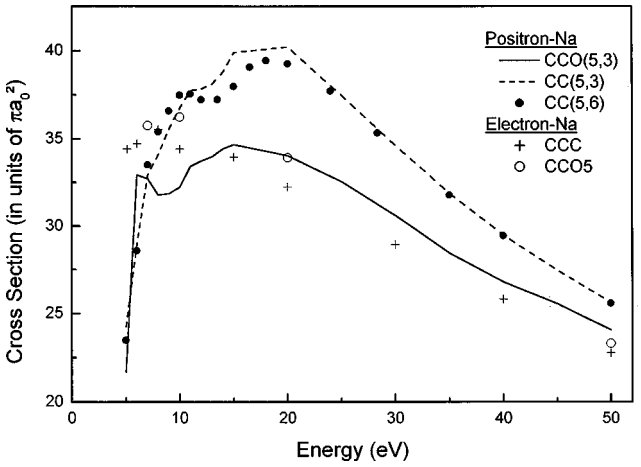

FIG. 5. $3s$-$3p$ transition cross section (in units of πa_0^2): the legends are the same as those in Fig. 4.

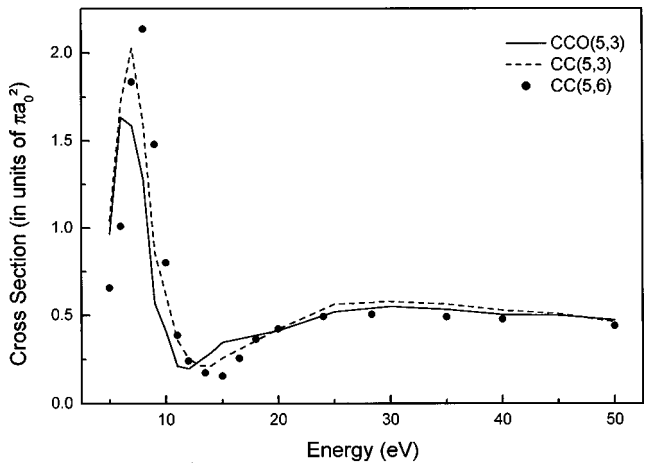

FIG. 6. $3s$-$4s$ Transition cross section (in units of πa_0^2): CCO(5,3) (——), CC(5,3) (– – –), and CC(5,6) (●).

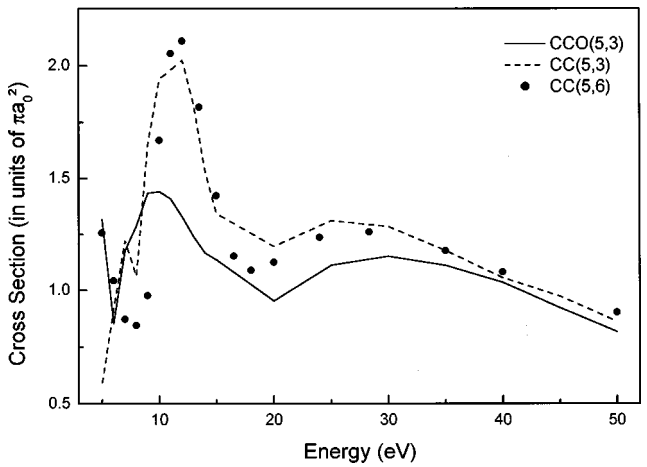

FIG. 8. $3s$-$4p$ transition cross section (in units of πa_0^2): the legends are the same as those in Fig. 6.

[19]. To study the similarities between the e^+-Na and e^--Na scattering system at the higher intermediate energies, we also include the CCC calculations of Bray [33] and CCO5 calculations for e^--Na scattering.

1. Elastic cross section

In Fig. 4 the elastic cross section for e^+-Na is depicted. It can be observed that the elastic cross section is a major contributor to the total cross section at the lower energies. For example, at 7 eV, the elastic cross section accounts for 30% of the total cross section but above 20 eV, the elastic cross section accounts for less than 15% of the total cross section. At the energy region of 10–12 eV, the CC(5,3) model displays the broad shoulder that has been similarly observed in the CC(5,6) calculations. It can also be seen that the CC(5,6) model agrees well with the CC(5,3) calculations.

Adding the optical potentials to the CC(5,3) calculations has quite an appreciable effect on the cross sections. The difference is especially obvious at the energy region between 10–15 eV where the broad shoulder was present for the pure CC calculations. We find that the CCO(5,3) is about 20–30% smaller than the CC(5,3) calculations in this energy region. The broad shoulder seen in the pure CC calculations is now reduced to a small structure for the CCO(5,3) model. It is highly plausible that the flux in this energy region is absorbed from the elastic cross section and materializes in the form of the ionization cross section, displaying the effect of the continuum in this transition. It must also be noted that the qualitative shape for this transition is similar to the other e^+–alkali-metal atom scattering calculations done by McAlinden and co-workers [20–22].

We have also depicted in Fig. 4, the CCC and CCO5 cross sections for the corresponding e^--Na scattering. It is gratifying to see that the differences between the CCC and CCO5 at 20 and 50 eV are within 15%. This illustrates that the optical potentials used in the small basis calculation CCO5 are probably modeling the continuum reasonably well.

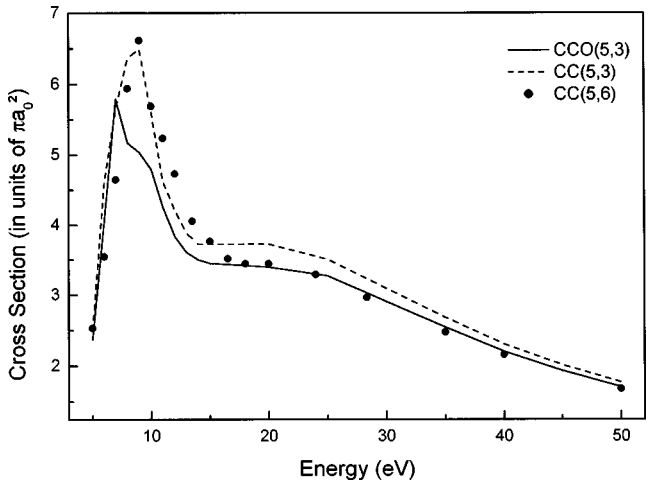

FIG. 7. $3s$-$3d$ transition cross section (in units of πa_0^2): the legends are the same as those in Fig. 6.

2. 3s-3p excitation cross section

In this transition (see Fig. 5) the cross section for the CC(5,3) model in this transition increases sharply from 6 to 10 eV, followed by a formation of a shoulder and a minima at the region of 12 eV and reaching a maximum at around 15 eV before decreasing again. It must be noted that the CC(5,6) calculations of Ryzhikh and Mitroy [19] also displays a shallow minima around 12 eV. At the higher energy range, this transition dominates. For example at 7, 10, and 50 eV, the contribution of this transition to the total cross section is about 35%, 50%, and 75%, respectively, for both the CC(5,3) and CCO(5,3) calculations.

Generally, the CCO(5,3) reduces the $3s$-$3p$ cross section quite appreciably above 6 eV. At 20 eV, the CCO(5,3) is smaller than the CC(5,3) models by about 17%. Furthermore, the ''shoulder'' seen in the CC(5,3) calculations at 12 eV undergoes changes with the implementation of the optical potentials. We also observe a structure in the region of 6–10-eV energy region. It has been seen that the qualitative shape of the $3s$-$3p$ transition is reminiscent of the $1s$-$2p$ transition in the e^+-H [27], the $2s$-$2p$ transition in the e^+-Li

[20], the $4s$-$4p$ transition in the e^+-K [22], the $5s$-$5p$ transition in the e^+-Rb, and the $6s$-$6p$ transition in the e^+-Cs scattering processes [21]. There is the possibility that in the present CCO(5,3), the qualitative shape of the structures may be enhanced with the continuum flux.

The CCC and CCO5 for the corresponding e^--Na system are also shown in Fig. 5 and we observe good agreement between the CCC and CCO5 at the two energies shown. This suggests that the optical potentials used are being modeled correctly. A simple five-state CC supplemented with continuum optical potentials is comparable to the 45-state CCC model of Bray [34]. Furthermore, the present CCO(5,3) shows good qualitative and quantitative agreement ($\approx$15%) with the CCC at $E>20$ eV. This provides an indirect proof that the physics of the e^+-Na and e^--Na may be quite similar at high energies.

3. 3*s*-4*s excitation cross section*

In general, the present CC(5,3) model shows qualitative similarities with the CCO(5,3) and the CC(5,6) data (refer to Fig. 6). Both the CC(5,3) and the CCO(5,3) models peak at 7 eV and reduce sharply to a minima before increasing gradually and tapering off. It can be seen that the addition of the optical potentials tend to reduce the peak observed at about 6–7 eV by 24%. Both the calculations tend to converge to each other at the higher energies. We also note that the general shape of the $3s$-$4s$ transition is quite similar to the $2s$-$3s$ transition in e^+-Li [20], the $4s$-$5s$ transition in e^+-K [22], the $5s$-$6s$ transition in e^+-Rb and the $6s$-$6p$ transition in e^+-Cs [21].

4. 3*s*-3*d excitation cross section*

The present CC(5,3) cross sections predict qualitatively similar cross sections as the CC(5,6) (see Fig. 7). However, with the addition of the optical potentials, the CCO(5,3) has a formation of a slight shoulder at 8 eV. The CCO(5,3) model has reduced cross sections when compared to the CC(5,3) model. Overall, the CCO(5,3) calculations show much similarity with the pure CC calculations.

5. 3*s*-4*p excitation cross section*

There are some differences between the CC(5,3) model and the CCO(5,3) model at the lower end of the energy region (see Fig. 8). The CC(5,3) displays a structure at 7 eV whereas the CCO(5,3) model is quite smooth. Again, similar to the other transitions, the CCO(5,3) model has reduced cross sections when compared to the CC(5,3) model almost throughout the entire energy region studied.

C. Total Ps formation cross section

The total Ps formation cross section is given as the sum of the transition from the ground state to Ps$(1s)$, Ps$(2s)$, and Ps$(2p)$. We also show the CC(5,6) cross sections as well as the experimental measurements of Zhou *et al.* [30] (see Fig. 9). In the work of Zhou *et al.*, the experimental measurements give an upper bound and a lower bound for the total Ps formation cross section. Overall, we find that the CC(5,3) and the CCO(5,3) models underestimate the lower limit of the total Ps formation experimental measurements by about 25% and 36%, respectively. The CC(5,6) model also underestimates the experimental measurements. It is also noted that the CC(5,6) has larger Ps formation cross sections than the CC(5,3) model, suggesting that convergence has not yet been achieved and calculations with larger Ps basis states need to be attempted.

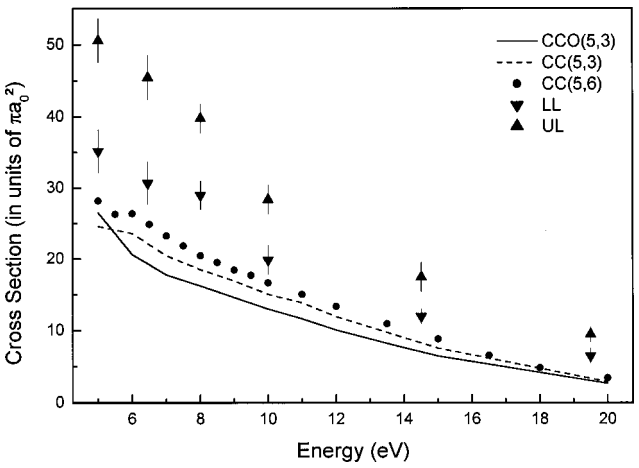

FIG. 9. Total Ps formation cross section (in units of πa_0^2): CCO(5,3) (——), CC(5,3) (– – –), CC(5,6) (●), and Zhou *et al.* [UL (▲) and LL (▼)].

D. Ionization cross section

In Fig. 10 we display the ionization cross section for the COPM and CCO(5,3) models. Due to the unavailability of experimental measurements of e^+-Na ionization cross sections, for comparative purposes we have included experimental measurements of Zapesochnyi and Aleksakhin [34] and Johnston and Burrow [32] for the ionization cross-section measurement of the e^--Na scattering process.

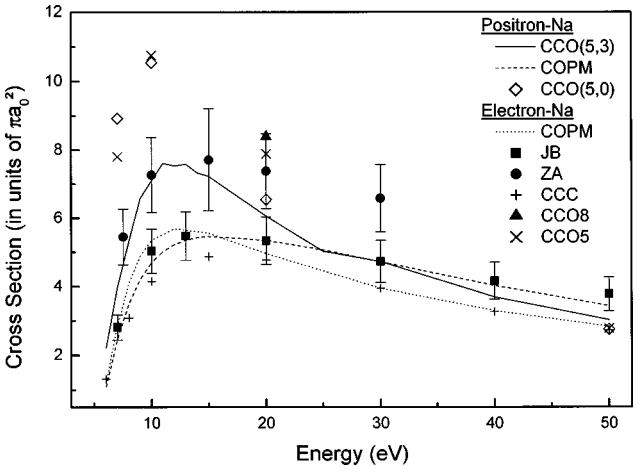

FIG. 10. Total ionization cross section (in units of πa_0^2): CCO(5,3) (——), COPM (e^+-Na) (– – –), CCO(5,0) (◇), COPM (e^--Na) (·····), Johnston and Burrow (■), Zapesochnyi and Aleksakhin (●), CCC (+), CCO8 (▲), and CCO5 (×).

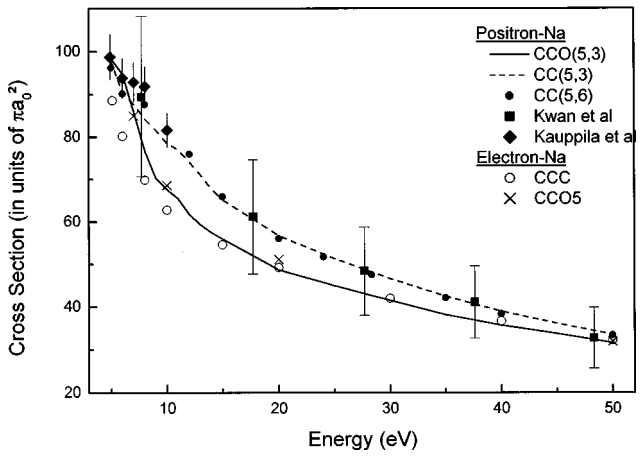

FIG. 11. Total cross section (in units of πa_0^2): CCO(5,3) (——), CC(5,3) (– – –), CC(5,6) (●), Kwan *et al.* (■), Kauppila *et al.* (◆), CCC (○), and CCO5 (×).

The current CCO5 calculations for the e^--Na scattering process agrees well with the earlier measurements of Zapesochnyi and Aleksakhin. We also note that the CCO8 work of McCarthy *et al.* [35] gave an ionization cross section of $8.4\pi a_0^2$, which is in good agreement with our CCO5 model (CCO5 predicts $7.9\pi a_0^2$). Of course, these CCO5 cross sections are larger than the CCC calculations and the COPM (e^-) for energies $E<20$ eV (see Fig. 10).

Similarly the CCO(5,3) calculations for e^+-Na are about 1.5 times larger than the COPM (e^+). It must also be noted that the COPM (e^+) and CCO(5,3) calculations do show signs of convergence at ten times the ionization threshold. These differences between the CCO(5,3) calculations and the COPM (e^+-Na) is quite puzzling. In the case of e^+-H scattering, Ratnavelu and Rajagopal [23] showed good agreement between their CCO models and the COPM. There could be many plausible reasons for these differences. One major factor may be due to the approximations used in the calculating the continuum optical potentials in a feasible manner but the good agreement between the COPM (e^--Na) and the CCC (see Fig. 1) provides much justification in our models. Again, we have the independent work of McCarthy *et al.* [35] using the CCO8 model for e^--Na that shows agreement with our CCO5 model. With these differences between the CCO(5,3) and the COPM (e^+-Na) for the ionization cross section, it would indeed be very helpful if e^+-Na ionization cross-section measurements and further theoretical calculations are done to resolve the observed discrepancies. We also note that the CCO(5,0) calculations for e^+-Na are up to 20% larger than the CCO(5,3) model, suggesting that the addition of higher Ps basis states might reduce the ionization cross section.

E. Total cross section

The total cross section for the present models are shown together with the CC(5,6) calculations of Ryzhikh and Mitroy (refer to Fig. 11). In addition, we also depict the e^--Na scattering calculations of the CCC model and the CCO5 calculations to see the convergence of the e^--Na and e^+-Na scattering calculations. Two different experimental measurements of Kwan *et al.* [28] and Kauppila *et al.* [29] have also been included. Both these measurements cannot discriminate against the elastic scattering from the forward direction. This will then reduce the measurements of the cross section by a magnitude equal to

$$\Delta\sigma_T = 2\pi\int_0^{\alpha} d\theta\,\sigma_{\rm el}(\theta)\sin\theta.$$

Therefore, it is necessary to apply a correction either to the experimental measurements or to the theoretical model. A correction to the experimental measurements seems more feasible and thus, the total cross section will be presented with corrections to the experimental measurements. In Fig. 11, the theoretical models are shown with the adjusted measurements of Kwan *et al.* [28] and Kauppila *et al.* [29], where we have added the elastic cross section up to an angle α from the CCO(5,3) calculations.

As can be observed in Fig. 11, both the CC(5,3) and CCO(5,3) models are within the experimental error bars of Kwan *et al.* [28]. This is not a good comparison since the experimental errors are quite large ($\approx$35%). On the other hand, the agreement with Kauppila *et al.* [29] is not good. We also note that the effect of the continuum on the total cross section where the CCO(5,3) is up to 15% smaller than the CC(5,3) model. To reduce the differences between theory and experiment, we believe that a CCOM calculation with larger Ps basis states and discrete atomic states should be attempted.

IV. CONCLUSION

In this work our objective was to study the e^+-Na scattering process at intermediate energies using the CCOM model and we have been successful in implementing the CCOM for the e^+-Na scattering process. As can be observed (using the present approximations), the continuum does seem to have quite an effect on the scattering process in the energy regime studied. Our results are quite comparable to the recent calculations of Ryzhikh and Mitroy [19] for most of the transitions studied.

Overall, the predicted total cross sections of the CCOM agree well with Kwan *et al.* [28] though due to the large error bars, these would not be seen as a stringent test to theoretical predictions. The quantitative agreement with the measurements of Kauppila *et al.* [29] is not as good in the region of 5–10 eV. We are quite sure that a definitive calculation is yet to be accomplished for e^+-Na scattering. Of course, there must be corresponding improvements in the experimental field to allow for a more discriminating test of the theories.

In the case of the total Ps formation cross section, the CCOM and the CC models consistently underestimate the experimental data of Zhou *et al.* [30]. It would also be desirable to reevaluate the experimental data for sodium since there is a large difference between the upper bound and the lower bound of the Ps formation. Ryzikh and Mitroy [19] have shown the dramatic effects in the higher excited cross

sections with the inclusion of higher Ps states. This should be explored in future studies with the implementation of the optical potentials.

Overall, the total ionization cross section of the CCO(5,3) model is small ($\approx$12%) compared to the total cross section, similar to the findings of McAlinden *et al.* [12] for e^+-Li. McAlinden *et al.* also suggested in their work that ionization is not a significant process. However, it can be seen in our work that the ionization channel has quite an effect on the other transitions, especially in the elastic and $3s$-$3p$ transitions (see Figs. 4 and 5), which are major contributors to the total cross section.

In the calculations of the total ionization cross section, there seems to be much discrepancies between the CCO(5,3) and the COPM (e^+) models. At the higher intermediate energies, the CCOM model shows convergence with the COPM. Nevertheless, we are quite perturbed with the discrepancies (that were not seen in the e^+-H case) [26,27]. Other theoretical calculations as well as experimental measurements of e^+-Na are greatly desired.

ACKNOWLEDGMENTS

K.R. would like to thank Dr. Jim Mitroy for the use of his close-coupling code. The financial support of the Malaysian Ministry of Science, Technology and Environment under the IRPA Project No. 09-02-03-0382 is also gratefully acknowledged. The authors would also like to thank Dr. Jim Mitroy and Dr. Igor Bray for providing data from their work. Part of the work was done by K.R. at the Department of Physics and Astronomy, University of Oklahoma. He wishes to acknowledge the financial support of the U.S. National Science Foundation through PHY-0071031 (under Professor Mike Morrison).

[1] I. E. McCarthy and A. T. Stelbovics, Phys. Rev. A **28**, 2693 (1983).
[2] B. H. Bransden, I. E. McCarthy, and A. T. Stelbovics, J. Phys. B **18**, 823 (1985).
[3] I. E. McCarthy, K. Ratnavelu, and Y. Zhou, J. Phys. B **26**, 2733 (1993).
[4] R. N. Hewitt, C. J. Noble, and B. H. Bransden, J. Phys. B **23**, 4185 (1990).
[5] J. Mitroy, J. Phys. B **26**, L625 (1993).
[6] J. Mitroy, Aust. J. Phys. **46**, 751 (1993).
[7] J. Mitroy, Aust. J. Phys. **48**, 646 (1995).
[8] J. Mitroy, Aust. J. Phys. **48**, 893 (1995).
[9] J. Mitroy, Aust. J. Phys. **49**, 919 (1996).
[10] K. Higgins and P. G. Burke, J. Phys. B **26**, 4269 (1993).
[11] J. Mitroy and A. T. Stelbovics, J. Phys. B **27**, 3257 (1994).
[12] M. T. McAlinden, A. A. Kernoghan, and H. R. J. Walters, Hyperfine Interact. **89**, 161 (1994).
[13] A. A. Kernoghan, M. T. McAlinden, and H. R. J. Walters, J. Phys. B **27**, L543 (1994).
[14] A. A. Kernoghan, M. T. McAlinden, and H. R. J. Walters, J. Phys. B **28**, 1079 (1995).
[15] A. A. Kernoghan, D. J. Robinson, M. T. McAlinden, and H. R. J. Walters, J. Phys. B **29**, 2089 (1996).
[16] K. Ratnavelu, J. Mitroy, and A. T. Stelbovics, J. Phys. B **29**, 2775 (1996).
[17] R. N. Hewitt, C. J. Noble, and B. H. Bransden, J. Phys. B **26**, 3661 (1993).
[18] J. Mitroy and K. Ratnavelu, Aust. J. Phys. **47**, 721 (1994).
[19] G. Ryzhikh and J. Mitroy, J. Phys. B **30**, 5545 (1997).
[20] M. T. McAlinden, A. A. Kernoghan, and H. R. J. Walters, J. Phys. B **30**, 1543 (1997).
[21] A. A. Kernoghan, M. T. McAlinden, and H. R. J. Walters, J. Phys. B **29**, 3971 (1996).
[22] M. T. McAlinden, A. A. Kernoghan, and H. R. J. Walters, J. Phys. B **29**, 555 (1996).
[23] H. Ray, P. Chaudhuri, and A. S. Ghosh, J. Phys. B **31**, 1631 (1998).
[24] K. D. Winkler, D. H. Madison, and I. Bray, J. Phys. B **32**, 1987 (1999).
[25] I. Bray, Phys. Rev. A **49**, 1066 (1994).
[26] K. Ratnavelu and K. K. Rajagopal, J. Phys. B **32**, L381 (1999).
[27] K. K. Rajagopal and K. Ratnavelu, Phys. Rev. A **62**, 022717 (2000).
[28] C. K. Kwan, W. E. Kauppila, R. A. Lukaszew, S. P. Parikh, T. S. Stein, Y. J. Wan, and M. S. Dababneh, Phys. Rev. A **44**, 1620 (1991).
[29] W. E. Kauppila, C. K. Kwan, T. S. Stein, and S. Zhou, J. Phys. B **27**, L551 (1994).
[30] S. Zhou, S. P. Parikh, W. E. Kauppila, C. K. Kwan, D. Lin, A. Surdutovich, and T. S. Stein, Phys. Rev. Lett. **73**, 236 (1994).
[31] K. K. Mukherjee, N. Ranjit Singh, K. B. Choudhury, and P. S. Mazumdar, Phys. Rev. A **46**, 234 (1992).
[32] A. R. Johnston and P. D. Burrow, Phys. Rev. A **51**, R1735 (1995).
[33] I. Bray, Phys. Rev. A **49**, R1 (1994).
[34] I. P. Zapesochnyi and I. S. Aleksakhin, Zh. Eksp. Teor. Fiz. **55**, 76 (1968) [Sov. Phys. JETP **28**, 41 (1969)].
[35] I. E. McCarthy, J. Mitroy, and R. Nicholson, J. Phys. B **24**, L449 (1991).